Chemistry & Biology
Article

Separate Entrance and Exit Portals for Ligand Traffic in *Mycobacterium tuberculosis* FabH

Sarbjot Sachdeva,[1,2,4] Faik N. Musayev,[2,4] Mamoun M. Alhamadsheh,[1,4] J. Neel Scarsdale,[3] H. Tonie Wright,[3] and Kevin A. Reynolds[1,*]
[1]Department of Chemistry, Portland State University, Portland, OR 97207, USA
[2]Department of Medicinal Chemistry
[3]Department of Biochemistry
Virginia Commonwealth University, Richmond, VA 23219, USA
[4]These authors contributed equally to this work.
*Correspondence: reynoldsk@pdx.edu
DOI 10.1016/j.chembiol.2008.03.007

SUMMARY

Mycobacterium tuberculosis **FabH initiates type II fatty acid synthase-catalyzed formation of the long chain (C_{16}–C_{22}) acyl-coenzyme A (CoA) precursors of mycolic acids, which are major constituents of the bacterial cell envelope. Crystal structures of *M. tuberculosis* FabH (mtFabH) show the substrate binding site to be a buried, extended L-shaped channel with only a single solvent access portal. Entrance of an acyl-CoA substrate through the solvent portal would require energetically unfavorable reptational threading of the substrate to its reactive position. Using a class of FabH inhibitors, we have tested an alternative hypothesis that FabH exists in an "open" form during substrate binding and product release, and a "closed" form in which catalysis and intermediate steps occur. This hypothesis is supported by mass spectrometric analysis of the product profile and crystal structures of complexes of mtFabH with these inhibitors.**

INTRODUCTION

The emergence of multidrug-resistant strains of *Mycobacterium tuberculosis* and the synergy of tuberculosis (TB) with AIDS have made TB one of the deadliest contemporary, infectious diseases, accounting for approximately 2–3 million deaths annually. The low permeability of the *M. tuberculosis* membrane (which plays a role in its intracellular survival) and its resistance to many chemotherapeutic agents (Jarlier and Nikaido, 1994; Nikaido and Jarlier, 1991) are conferred by the long chain α-alkyl-β-hydroxy fatty acids (mycolic acids) that constitute approximately 50% of the weight of the lipid-rich cell envelope of the bacterium. The frontline antitubercular drug isoniazid targets InhA, an enzyme required for mycolic acid biosynthesis (Rozwarski et al., 1998; Larsen et al., 2002), and other enzymes in the essential fatty acid biosynthetic pathway are also attractive targets for new TB-therapeutic agents.

Mycolic acids are formed through the sequential activities of type I and type II fatty acid synthases (FASs) (Asselineau et al., 2002). The type I FAS is a homodimer of a multifunctional polypeptide that carries all of the catalytic activities for de novo synthesis of coenzyme A (CoA)-linked C_{16}–C_{26} long chain fatty acids. Further elongation to C_{56} meromycolic acids is proposed to be carried out by a type II FAS, the multiple catalytic activities of which are each associated with separate polypeptides that utilize acyl carrier protein (ACP) as shuttle in the extension cycle. Mycolic acids are formed through condensation of these meromycolic acids with long chain fatty acids (Portevin et al., 2004; Takayama et al., 2005).

M. tuberculosis FabH (mtFabH), the initiator enzyme of the type II FAS, is an important link between the FAS types I and II (Scarsdale et al., 2001; Choi et al., 2000b). It catalyzes a decarboxylative condensation of the long chain (C_{16}–C_{22}) acyl-CoA products of the type I FAS-catalyzed reaction with malonyl-ACP. The resulting 3-ketoacyl-ACP product is reduced to an acyl-ACP (extended by two carbons) through the action of three enzymes (one of which is InhA) (Figure 1; Sacco et al., 2007a, 2007b; Brown et al., 2007). This acyl-ACP is further elongated in subsequent steps catalyzed by KasA and KasB (Bhatt et al., 2007; Sridharan et al., 2007). mtFabH can utilize a wide range of C_{12}–C_{22} acyl-CoA substrates (Scarsdale et al., 2001; Choi et al., 2000b; Brown et al., 2005), which distinguishes it from FabH in other type II FAS systems that typically utilize C_2–C_6 substrates (Han et al., 1998; Choi et al., 2000a).

The catalytic cycle of homodimeric mtFabH initiates with binding of acyl-CoA substrate followed by acylation of the active site cysteine to form a thioester and dissociation of CoA. The carbonyl oxygen of the acylthioester intermediate is stabilized in an oxyanion hole by main chain –NH– proton donors Cys112 and Ala306 (see Scarsdale et al., 2001 for mtFabH numbering); the acyl group lies in a "closed" channel that can accommodate chains up to C_{16} in length. Malonyl-ACP then binds in the vacated CoA binding site where the malonyl carboxylate is stabilized in an anion binding pocket consisting of His244 and Asn274. These residues also contribute to catalysis of the malonyl-ACP decarboxylation to form a carbanion, which reacts with the acyl group in the thioester to form 3-ketoacyl ACP, the released product of the reaction.

The crystal structure of the Michaelis complex of lauroyl-CoA with an inactive Cys112Ala mtFabH mutant (Musayev et al., 2005) clearly shows substrate bound in an "L"-shaped channel of each monomer (Figure 1), with the active site triad

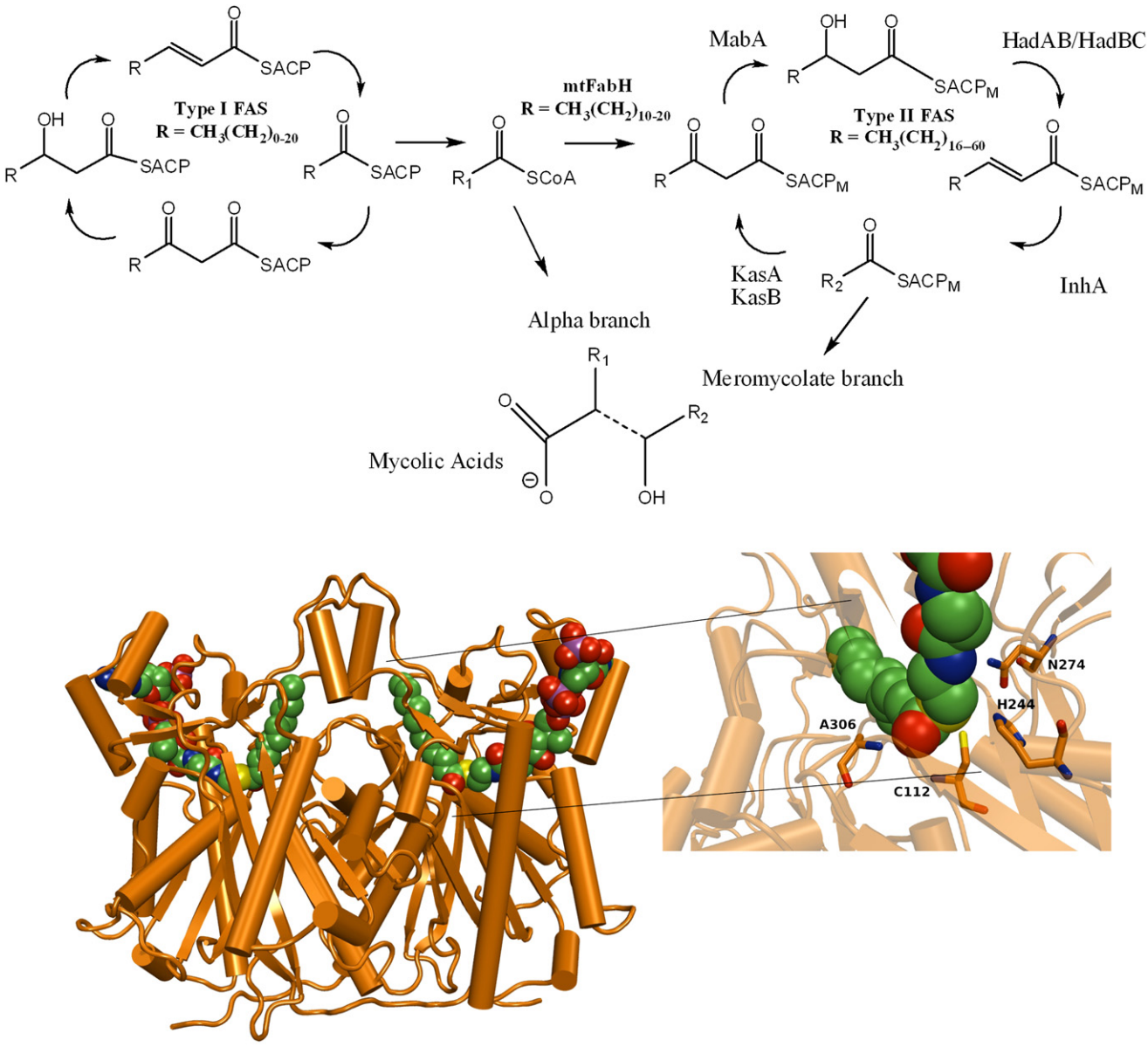

Figure 1. Structure and Proposed Biological Role of mtFabH

Top panel: FabH as a link between the type I and type II FAS pathways of *M. tuberculosis*.

Bottom panel: backbone structure of Cys112Ala mtFabH homodimer (gold ribbon) in complex with lauroyl-CoA (space filling: green = carbon; red = oxygen; blue = nitrogen; yellow = sulfur; magenta = phosphorous) bound in the buried, L-shaped binding site of each monomer of the dimer. Also shown is an expansion of active site residues (gold stick) with functional atoms (color coded as before) and Cys112 modeled from WT mtFabH structure for the lauroyl-CoA.

(Cys112-His244-Asn274) at the junction of the two arms of the L (Figure 1). CoA occupies the solvent accessible pantetheinate arm of the L, while the acyl group occupies the distal, dead-end arm of the L, an extended hydrophobic channel that appears accessible only through the pantetheinate channel. Binding of lauroyl-CoA substrate would thus appear to require migration of the hydrophobic lauroyl chain through the pantetheinate binding channel and around the bend of the L past the hydrophilic and charged catalytic residues. Formation of the complex in this manner would present formidable stereochemical and energetic barriers, and dissociation of long chain β-ketoacyl-ACP reaction product from this buried hydrophobic site via a reversal of this process would appear to be equally unfavorable.

These considerations have led us to hypothesize that native mtFabH adopts a hitherto unobserved "open" conformation, which offers an alternate pathway with lower energy barriers for initial substrate binding and final product release. To test this hypothesis, we prepared inhibitors with hydrophobic arms that occupy one or both binding channels, and a reactive group that targets the active site cysteine. The binding modes of these inhibitors with the wild-type (WT) mtFabH have been established by mass spectrometry and X-ray crystallography. These same

analyses with an mtFabH Ala246Phe mutant, the pantetheinate binding channel of which is blocked, reveal that inhibitor binding and reaction still proceed efficiently, but only with one-armed inhibitors that bind exclusively in the acyl channel. These experiments provide strong evidence that mtFabH exists in an open conformation that accepts ligands directly into the acyl binding channel without entry to the single solvent portal and passage through the pantetheinate channel of the closed form of the enzyme. These results support a new model for substrate binding, catalysis, and product release in mtFabH.

RESULTS

Inhibitor Design and Activity

We have recently demonstrated that alkyl-CoA disulfide inhibitors target the active site cysteine of both ecFabH and mtFabH and that inhibition of these enzymes is specific for short (C_2) or long (C_{10}) alkyl chains respectively, matching their acyl chain substrate specificities (Alhamadsheh et al., 2007). To investigate the route for ligand binding and reaction with mtFabH, we synthesized linear inhibitors (Figure 2, compounds **1**–**3**) composed of two arms linked by an oxycarbonyl-disulfide group, which can potentially react with the reactive site Cys112 by acylation or by thiol-disulfide exchange. The arms in the compounds used here are ethanol and decyl and decanoic acid. Each pair of arms of a compound is potentially able to simultaneously bind in the acyl and pantetheinate binding channels of mtFabH. Preliminary analysis under standard conditions (Alhamadsheh et al., 2007) revealed comparable levels of inhibition for mtFabH (IC_{50} values: **1**, 3.8 ± 0.5 μM; **2**, 2.4 ± 0.8 μM; **3**, 2.7 ± 0.2 μM).

Reaction Products and Crystal Structures of mtFabH and C112A mtFabH with 1

Electrospray ionization mass spectrometry (ESI-MS) was used to follow modification of the WT mtFabH with an excess of **1**. Under these conditions, the protein was completely modified (Figure 2, top panel), the two major species exhibiting mass increases of either 230 or 338 Da. The former of these is consistent with addition of three 77 Da fragments of A (theoretical increase in mass of 231 Da) to mtFabH monomer, while the latter is consistent with addition of two 77 Da fragments of A and one 185 Da fragment of B (theoretical increase in mass of 339). These analyses indicated that all three solvent-accessible cysteines in WT mtFabH (the active site Cys112, plus Cys23 and Cys154) can react with **1** through disulfide exchange and at least one can react through acylation.

Crystallization of preformed inhibition complex (Table 1) of WT mtFabH with **1** showed extra electron density at the two surface cysteines (Cys23 and Cys154), consistent with disulfide-linked β-mercaptoethanols, and at the active site Cys112, consistent with acylation by the long B arm fragment of **1**. This crystal structure corresponds to the more abundant trimodified reaction product denoted (A+A+B) identified by mass spectroscopy. The contiguous electron density in both mtFabH subunits extending from the active site Cys112 into both acyl and pantetheinate binding channels (Figure 3A) was interpreted and successfully refined as dual, conditional half occupancy of each channel by fragment B of compound **1**, the carbonyl carbon of which forms a thioester with the active site Cys112 sidechain −SH.

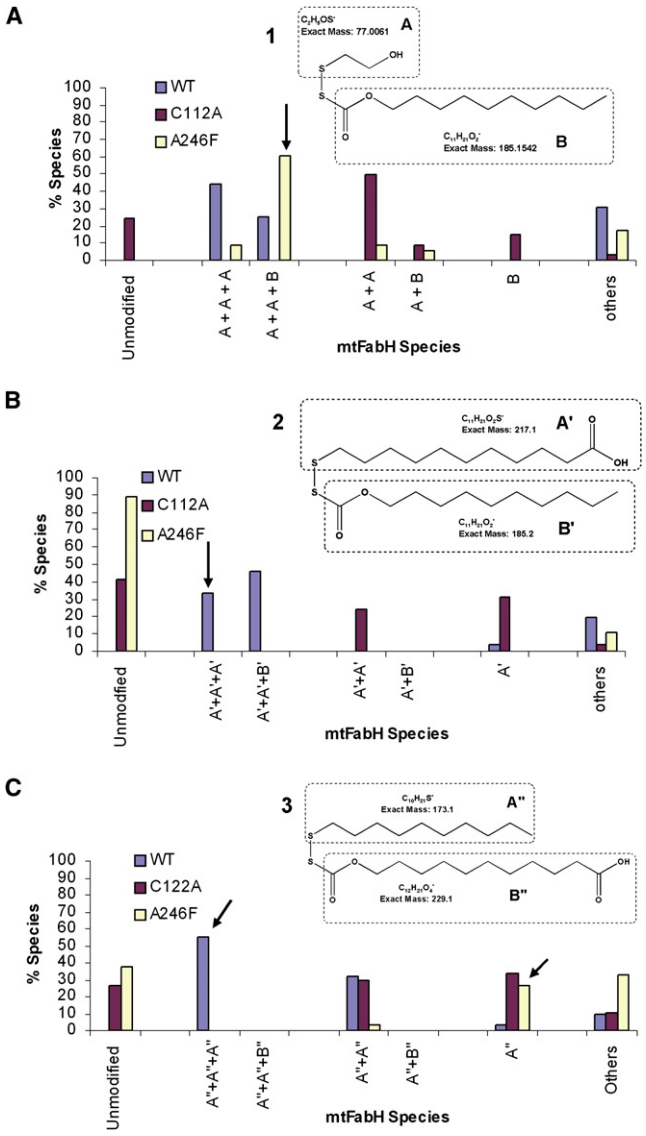

Figure 2. ESI-MS Analyses of the Product Abundances for the Reactions of Disulfide Inhibitors with the mfFabH

Adducts made between compounds **1** (A), **2** (B), and **3** (C) with the WT (blue bars), Cys112Ala (maroon bars), and Ala246Phe (yellow bars) mtFabH are shown. Reaction products are grouped in descending order of substitution, as noted along the x axis. Arrows indicate species for which a crystal structure was obtained.

The carbonyl oxygen of the thioester-linked fragment B makes different hydrogen bonding interactions with the protein in its alternate orientations in the acyl and pantetheinate channels of each mtFabH monomer subunit. Furthermore, fragment B in the acyl (or pantetheinate) channel of one FabH monomer differs from that of its counterpart in the same channel of the other monomer of the asymmetric unit dimer. Consequently, there are four distinct local environments of the carbonyl group in the asymmetric unit. The carbonyl oxygen of fragment B in both acyl channels of the dimer makes a hydrogen bond to the main chain −NH− of Ala306, but not to the −NH− of Cys112. However, in one subunit, this carbonyl oxygen makes a long

Table 1. Crystallization Conditions for Inhibitor Complex Structures Determined

Inhibitors[a]	Protein	Protein Concentration (mM)	Protein:Inhibitor Molar Ratio	Reservoir Solution	Lattice Parameters A (Space Group)	Accession No.
1	Wt	0.21	1:3.5	50 mM Na acetate, pH 4.6, 2.4 M Na formate	68.03, 88.85, 229.74 ($C222_1$)	2QNZ
1	A246F	0.11	1:4	100 mM Na Hepes, pH 7.5, 1 M K/Na tartrate	67.70, 88.69, 229.90 ($C222_1$)	2QNY
2	Wt	0.15	1:5	100 mM Na Mes, pH 6.5, 50 mM NaH_2PO_4/KH_2PO_4, 1.8 M NaCl	68.28, 88.98, 230.25 ($C222_1$)	2QNX
3	Wt	0.4	1:2.5	100 mM Na Hepes, pH 7.5, 1 M K/Na tartrate	68.41, 89.12, 233.29 ($C222_1$)	2QO1
3	A246F	0.21	1:4	100 mM Na citrate, pH 5.6, 10% isopropanol, 18% PEG-4K	55.30, 93.05, 104.72 ($P2_12_12_1$)	2QO0

[a] See Figure 2.

hydrogen bond to the side chain of Ser276, while, in the other subunit, the Ser276 side chain has alternate conformations, both of which make favorable (2.6 Å) hydrogen bonds to the ester, but not to the carbonyl oxygen, of the ligand in the acyl channel. These hydrogen bonds to the Ser276 side chain −OH may compensate for the absence of the hydrogen bond to the main chain −NH− of Cys112 in the oxyanion hole.

The carbonyl oxygen of fragment B bound in the pantetheinate channel of one subunit makes a hydrogen bond with the side chain $-NH_2$ of Asn274 (3 Å) but not to His244, the two residues that constitute the malonyl anion binding site. In the second subunit, the carbonyl oxygen of fragment B bound in the pantetheinate channel makes tenuously long hydrogen bonds (3.3 Å and 3.6 Å, respectively) to these groups in the malonyl anion site, but makes a favorable hydrogen bond (2.5 Å) to the side chain of Ser276 in one of its two alternate conformations.

ESI-MS analyses of the Cys112Ala mutant complex prepared under the same conditions showed no trimodified species (Figure 2, top panel). Instead, a predominant dimodified species (mass increase of 152 Da) was observed, consistent with addition of two 77 Da fragments of A. Two less abundant species were also observed (mono- and dimodified), consistent with the addition of a single B fragment and an A+B, respectively, that together approximated the unmodified species in abundance (Figure 2, top panel). This decrease in the number of cysteine modifications coincident with mutation of the active site Cys112 indicates that it is this residue in the WT mtFabH that can undergo modification with either fragment A or B.

Reaction of A246F mtFabH with 1

The alternate occupancy of the acyl and pantetheinate channels of WT mtFabH by the $C_{10}H_{21}OCO$ (B fragment) groups in the above structures could be realized by two binding orientations of **1** prior to reaction with the active site Cys112. The alternate occupancy might also arise if there were only one binding orientation that permitted reaction with C112, with a subsequent equilibration of the covalently linked $C_{10}H_{21}OCO$ chain between the two channels. In either case, migration of the inhibitor into the pantetheinate channel with passage through the active site residues into the acyl channel presents similar formidable energetic barriers to those facing the natural acyl-CoA substrate. Thus, we considered that there may be alternative modes for substrate and ligand entry to the extended mtFabH binding site.

To test this hypothesis, we created an Ala246Phe mutant mtFabH, which introduces a large obstructive group into the pantetheinate channel about 8–9 Å out from the active site Cys112. This Ala246Phe mtFabH mutant had no detectable catalytic activity in an elongation assay with lauroyl-CoA and malonyl-ACP. Mass spectrometry (Figure 2, top panel) revealed that an incubation of **1** with this Ala246Phe mutant resulted in the same trimodification seen with the WT enzyme. Both trimodified species (A+A+A and A+A+B) were observed, with an apparent greater abundance of the latter.

The crystal structure of the unliganded Ala246Phe mutant showed no significant differences in structure relative to the WT except for the presence of the bulky phenylalanine, which clearly blocks access to the active site cysteine via the pantetheinate channel. Electron density was observed in the acyl channel that can be fit with a free laurate (not linked to the active site cysteine). Like other mtFabH structures crystallized in the absence of ligands, including the WT, the electron density in the acyl channel that can be fit with a free laurate is probably taken up during expression and purification of the recombinant mtFabH.

The cocrystal structure of Ala246Phe mtFabH with **1** (Figure 3B) shows the overall structure of the protein to be virtually identical to that of the unliganded mutant. The hydrophobic ligand, modeled as laurate in the acyl binding channel of the unliganded Ala246Phe crystal structure, is replaced in the liganded form by electron density contiguous with Cys112 that can be well fit by fragment B of **1** in thioester linkage with Cys112 (Figure 3B). There was no ligand electron density in the blocked pantetheinate channel. The carbonyl group of B in the Ala246Phe mtFabH complex assumes two alternate orientations, one toward the oxyanion hole and the other toward the malonyl anion binding site. In one subunit, the carbonyl oxygen makes hydrogen bonds with optimal stereochemistry to −NH− of Cys112 and Ala306 in the oxyanion hole of the acyl binding site. In the other subunit, the hydrogen bond to −NH− of C112 is too long to be significant, and the ligand interactions resemble those seen in the WT complex. In both subunits of the dimer of the Ala246Phe ligand complex, the alternative conformation of the carbonyl oriented toward the malonyl anion binding site positions the oxygen

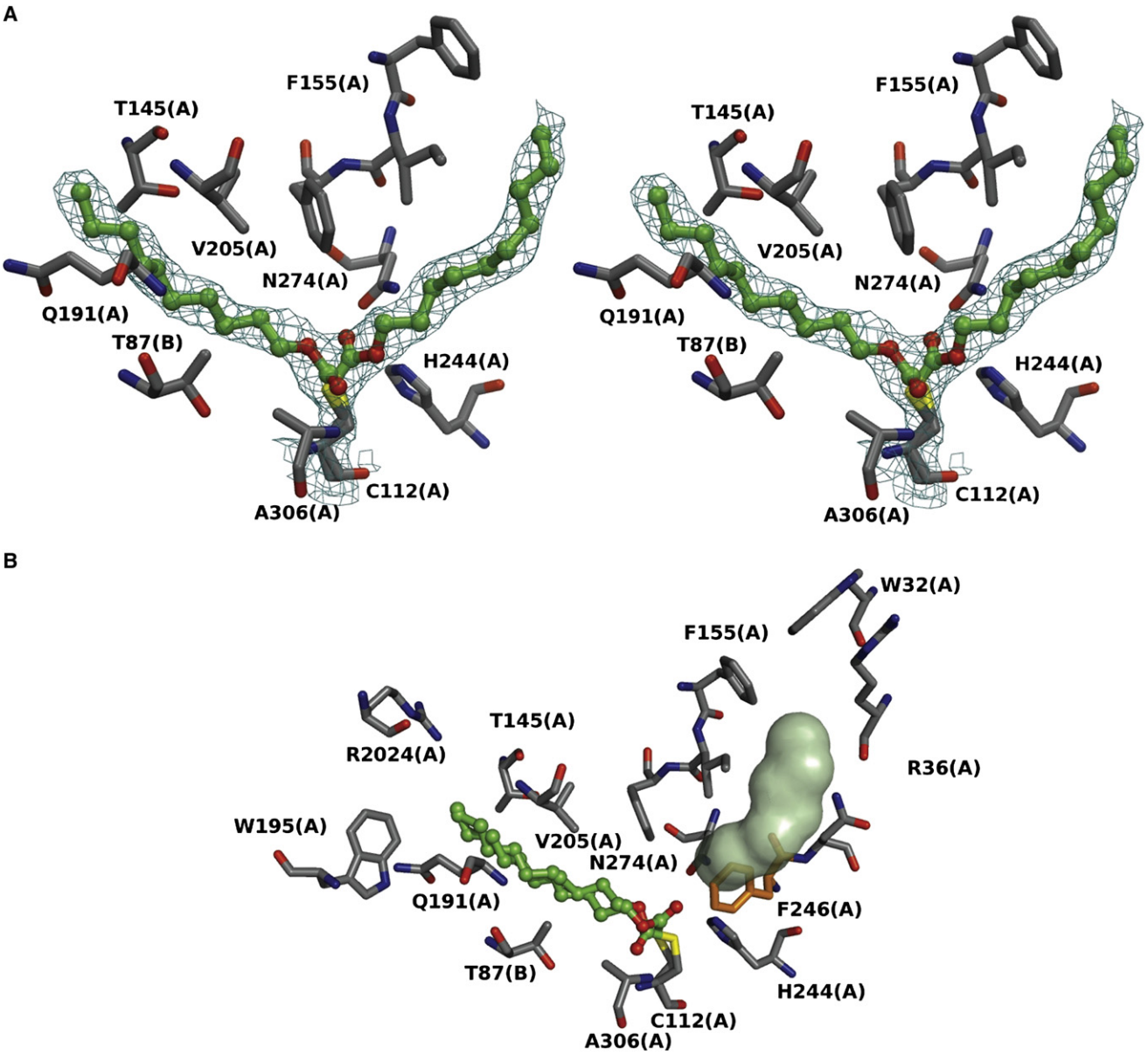

Figure 3. View of the Product Structure of Compound 1 in the Binding Channels of the WT and Ala246Phe Mutant

(A) Stereo view of the WT mtFabH, showing fragment B of its electron density alternately bound in each of the two arms, the acyl channel and the pantetheinate channel, of the substrate binding site. The map is 2mFo-DFc contoured at 1σ. Subunits of the dimeric mtFabH are indicated by the A and B suffix.

(B) Structure of the Ala246Phe mutant with the pantetheinate channel (gray space filling surface) access to the active site cysteine blocked by a phenylalanine residue and fragment B (2 conformations) of compound **1** bound in the acyl channel.

at long hydrogen bond distance from the His244 and Asn274 proton donors.

The vacant pantetheinate channel in the Ala246Phe mutant confirms that this channel is blocked by the phenylalanine mutation and indicates that **1** must enter the acyl binding channel by a path other than the pantetheinate channel. We hypothesize that this alternative path exists in an open form of the enzyme in which the extended binding site, consisting of the two channels, is accessible to ingress of the inhibitor as a result of the lifting of a loop that covers both binding channels (see Discussion below).

Reaction of mtFabH, Cys112Ala mtFabH, and Ala246Phe mtFabH with 2 and 3

Inhibitor **1** contains only one long hydrophobic arm, which, as shown above, can occupy either channel of WT mtFabH, or just the acyl binding channel of the Ala246Phe mutant. To determine the accessibility to the binding sites of the several FabH forms, we synthesized **2** and **3** (see Figure 2 for structures), both with two long arms differing only in the addition of a carboxylate group to the C_{10} alkane chain. These inhibitors with two hydrophobic arms are, in principle, competent to bind both channels of the active site. In addition to providing potential full

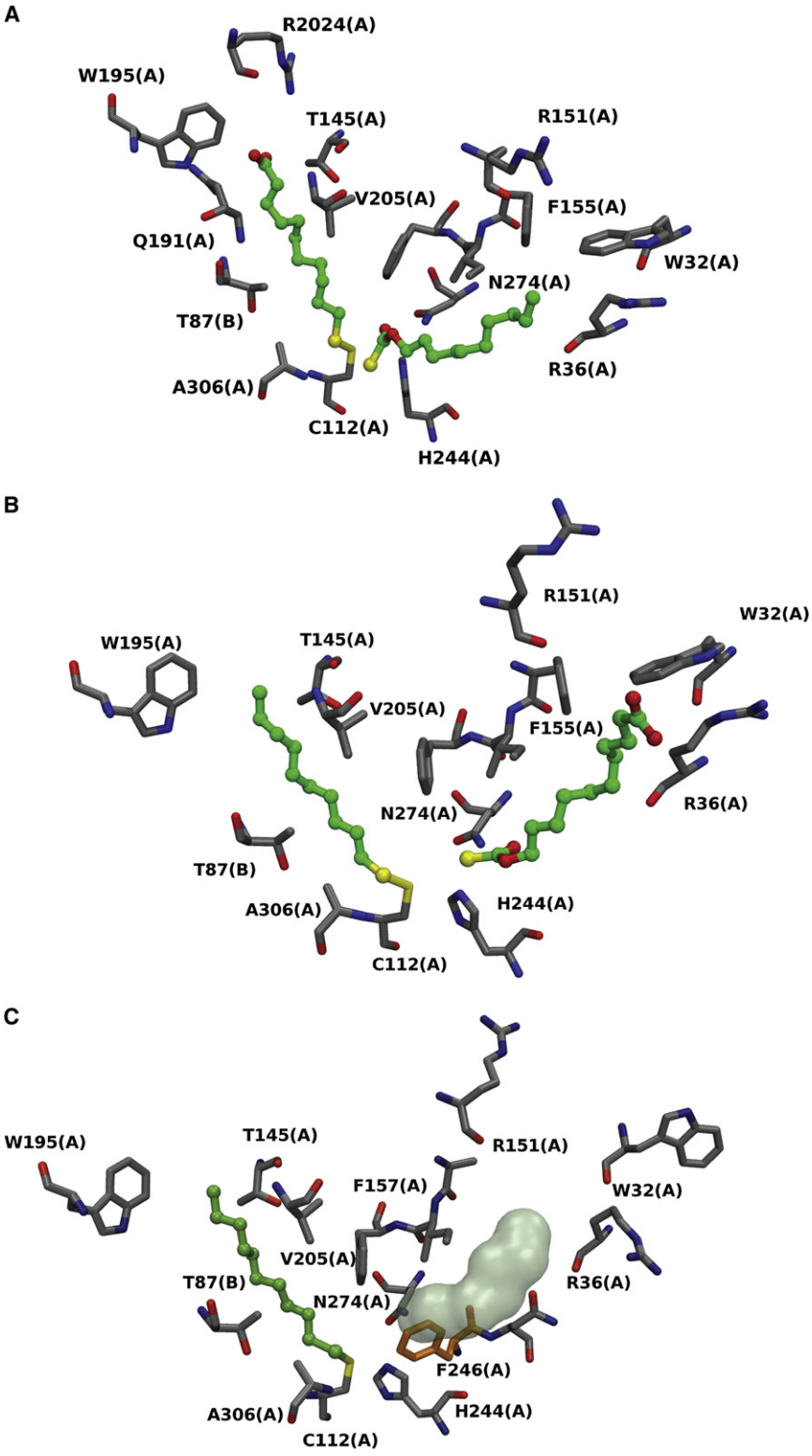

Figure 4. Structure of Products of Compounds 2 and 3 with WT and Ala246Phe mtFabH

(A) Structure of the product of compound **2** with mtFabH showing fragment A′ in the acyl channel disulfide linked to Cys112, and fragment B′ in the pantetheinate channel. Arrows identify the acyl channel and pantetheinate channel. Subunits of the dimeric mtFabH are indicated by the A and B suffix.

(B) Structure of the product of compound **3** with WT mtFabH showing fragment A″ in the acyl channel disulfide linked to Cys112 and fragment B″ in the pantetheinate channel.

(C) Structure of the product complex of compound **3** with Ala246Phe mtFabH showing fragment A″ in the acyl channel disulfide linked to Cys112. The surface shape of the empty pantetheinate channel is shown blocked by Phe246.

occupancy of both channels of the enzyme, the anionic carboxylate of **2** and **3** was expected to both inhibit the putative transit of the long chain through the pantetheinate channel and into the acyl channel, and to direct ligand orientation according to the relative hydrophobicities of the two inhibitor arms and the two arms of the binding channel.

The reaction of WT mtFabH with **2** (Figure 2, middle panel) resulted in two trimodified products with mass increases of either 617 or 648 Da. The lower mass increase is consistent with addition of two 217 Da A′ fragments and one 185 Da B′ fragment, while the higher mass increase is consistent with addition of three 217 Da A′ fragments (an overall increase in theoretical mass of 619 or 651 Da, respectively) per mtFabH monomer. There was no detectable unmodified protein. Reaction of **3** with WT mtFabH gave predominantly trimodified products exclusively with A″ chain fragment (some A″ + A″ dimodified species were also observed).

Crystal structures of the WT enzyme with **2** and **3** showed that, in both cases, a disulfide species was formed between the A′ or A″ fragments and the active site Cys112 (Figures 4A and 4B). In the structure of WT mtFabH with **2**, the undecanoic acid group is, surprisingly, in the acyl channel and the *O*-undecylcarbonothioate lies in the pantetheinate channel, detached from the C112-disulfide-linked undecanoic acid and with its carbonyl oxygen oriented toward the malonyl anion binding site of His244 and Asn274 (Figure 4A). Hydrogen bonds in this binding site are close to optimal in one subunit (2.72 and 2.74 Å), but are long in the other subunit (3.34 and 3.45 Å). The crystal structure of WT mtFabH complexed with **3** (Figure 4B) shows the decyl chain in the acyl channel disulfide linked to Cys112. The *O*-carboxyundecylcarbonothioate in the

pantetheinate channel is present in the same orientation as the *O*-undecylcarbonothioate group in the complex with **2**, with its carboxylate at the mouth of the pantetheinate channel and its carbonyl oriented toward the malonyl anion binding site, but too far from His244 and Asn274 in both subunits to make hydrogen bonds. This latter difference, vis a vis the complex with **2**, may be a consequence of lattice interactions of the carboxylate that are transmitted to the other end of the chain in the malonyl anion binding site.

These observations demonstrate that the linkage positions of the undecanoic acid chain and the decyl chain in **2** and **3** do not determine the orientation of binding these compounds in the acyl site of mtFabH. For **2**, the binding of the undecanoic acid in the acyl binding channel is possibly stabilized by the presence of the Arg2024 side chain at the top of the acyl channel in both subunits (4–5 Å from the carboxylate). In one subunit, there is also a hydrogen bond between one of the carboxylate oxygens (inferred to be in the protonated state) and the amido oxygen of the side chain of Gln191. The recurrence of disulfide exchange products in both cases where the inhibitor has two long arms suggests that orientation in binding is determined primarily by the positioning of the oxycarbonyl-disulfide group in the active site. The crystal structures show that the carbonyl oxygen of this group is directed toward the malonyl anion binding site, and this may be the principal determinant of ligand orientation. For a mechanism involving transit through the pantetheinate into the acyl channel, there is no obvious basis for discrimination in the orientation of the oxycarbonyl-disulfide group. This and the presence of the carboxylate in the acyl channel argue against a threaded transit of the ligand into its final reactive position and for a lower energy pathway of entry.

Reaction of **2** and **3** with the Cys112Ala and Ala246Phe mutants leads to no detectable trimodification of the protein (Figure 2, middle and bottom panels). For both inhibitors **2** and **3**, a predominant reaction product species was the unmodified mutated proteins. These results contrast with those of the WT FabH, where there was no unmodified protein and the major species observed with either inhibitor was the trimodified species. A striking observation from these ESI-MS studies is that the Ala246Phe mutant behaves like the Cys112Ala mutant with **2** and **3**, but like the WT mtFabH with **1**. The presence of the phenylalanine mutation dramatically affects reaction of the active site cysteine, but only with inhibitors having two hydrophobic arms.

A cocrystallization study of **3** with the Ala246Phe mutant revealed a complex with the A″ fragment linked by a disulfide to Cys112 and lying in the acyl channel like the ligand complexes with WT mtFabH (Figure 4C). Fragment B″, which is observed in the pantetheinate channel of WT mtFabH, is absent in this Ala246Phe mutant, and this channel remains blocked by the phenylalanine mutation (Figure 4C). Thus, while the ESI-MS results indicate that efficient reaction of the active site cysteine with **3** is compromised by this mutation, the crystal structure shows that the reaction occurs. These different results may be due to differences in conditions of preparation of the samples used for mass spectrometry and for crystallization. Nevertheless, formation of the product complex of **3** with the Ala246Phe mutant by entry of **3** through the pantetheinate channel, which is blocked, seems unlikely. The most parsimonious hypothesis for its formation is that **3** binds to an open form of the enzyme through interaction of its oxycarbonyl-disulfide group at the malonyl anion binding site; this orients A″ in the acyl channel for disulfide exchange with Cys112, while B″ extends into solvent from the open form in lieu of binding in the pantetheinate channel, and dissociates when the thiol-disulfide exchange reaction occurs.

DISCUSSION

Unresolved Aspects of *M. tuberculosis* FAS II Enzyme Mechanisms

The *M. tuberculosis* type II FAS pathway for synthesis of long chain (>C_{54}) fatty acid precursors of the mycolic acid component of the bacterial cell wall (Lu et al., 2004) is a proven target for existing TB treatments and offers other opportunities for development of new treatments. Binding and transfer of long chain acyl reactants and products almost certainly require enzyme conformational changes and specific protein-protein interactions, some of which may be vulnerable points for therapeutic development. In particular, it is not clear how some well-characterized enzymes of this pathway can accommodate substrates of widely variable acyl chain length and how the protein components of the pathway interact.

Characterization and structure determination of individual enzymes (Rozwarski et al., 1998; Scarsdale et al., 2001; Sridharan et al., 2007; Cohen-Gonsaud et al., 2002, 2005) and ACP (Wong et al., 2002) in this pathway provide evidence that conformational changes of the proteins play an important role in some individual steps. For instance, conformational changes on substrate binding to InhA (FabI) provide an accessible acyl binding crevice to which a C_{16} $\Delta^{2,3}$-dodecenoic thioester binds in a U-shaped conformation (Rozwarski et al., 1998). For the reductive enzyme 3-ketoacyl reductase (MabA), open and closed forms of the enzyme have been observed, and docking studies suggest that an L-shaped binding pocket in the open form can accommodate substrates up to C_{16} (Cohen-Gonsaud et al., 2002, 2005); however, it is unclear how physiological substrates with acyl chains longer than C_{16} bind to either InhA or MabA. An acyl binding region for C_{10} and C_{12} substrates in the condensing enzyme mtKasB has been identified and is U-shaped. While this binding pocket is larger and more occluded than the corresponding binding region of the *Escherichia coli* FabB (which catalyzes the analogous reaction during palmitate biosynthesis in this microorganism) (Sridharan et al., 2007), there are no data suggesting how the much longer physiological substrates bind to mtKasB.

There is less information on protein-protein interactions in the *M. tuberculosis* type II FAS, but there is evidence that such interactions are essential for mycobacterial viability (Veyron-Churlet et al., 2005, 2004). Formation of a type II FAS complex, possibly with some features resembling those in the type I FAS (Jenni et al., 2007; Lomakin et al., 2007), is likely required to facilitate passage of the extremely long chain fatty acid substrates between enzymes.

To date, there is no information on conformational changes or protein-protein interactions of mtFabH. The linear acyl binding pocket appears to be capable of accepting substrates only up to about C_{16} in length (Scarsdale et al., 2001), while experiments

have shown that the enzyme can process C_{22} substrates (Brown et al., 2005). The crystal structure of mtFabH also raises the question of how substrate (and product) enter (and leave) the extended L-shaped binding site consisting of two long, tandem channels, which are roughly perpendicular to each other. The distal, buried acyl binding channel in the mtFabH structure appears accessible only through the pantetheinate channel, which opens to solvent. However, a binding process in which lauroyl- or other long-chain acyl-CoA is threaded first through the pantetheinate channel into the acyl channel seems implausible.

A Model for Substrate Binding and Product Release in mtFabH

An alternative to this substrate-threading model is a mechanism in which mtFabH exists in an open conformational state, where both the acyl and pantetheinate binding channels are accessible. To test this hypothesis, we used active site-directed oxycarbonyl-disulfide inhibitor ligands flanked on each side by alkyl or carboxyalkyl chains. Since existing crystal structures of both liganded and unliganded mtFabH are inferred to be in the closed conformational state of the enzyme, we combined solution ESI-MS and crystal structure data to analyze the reaction pathways and product complexes of these inhibitor ligands with mtFabH. These results provide evidence that these compounds do not bind to mtFabH by passage through the pantetheinate channel into the acyl channel. Inhibitor **1** efficiently enters the acyl channel of the mtFabH Ala246Phe mutant, blocked in the pantetheinate channel, and the carboxylated C_{10} arm of compound **2** binds in the acyl channel of WT mtFabH despite the inferred energetic obstacle to migration of a polar group through two hydrophobic channels. These data argue strongly for an open form of mtFabH that binds acyl substrates or inhibitors.

A crystal structure of a disordered ecFabH (Qiu et al., 2001), and recent kinetic data for inhibition of this enzyme with alkyl-CoA disulfide inhibitors (Alhamadsheh et al., 2007), support a model in which the open dimeric enzyme becomes ordered on binding of an acetyl-CoA substrate or methyl-CoA disulfide inhibitor. There is no experimental crystal structure in a disordered or open form for mtFabH, and a large structural change in the observed closed crystal structure would be required to provide direct access to the long hydrophobic acyl channel. Inspection of the mtFabH structure reveals that the extended binding site of this enzyme could be exposed for concerted binding of long chain acyl-CoA substrates through movement of a single polypeptide segment (residues 183–209, ecFabH numbering), which forms most of the top of the acyl channel and part of the top of the pantetheinate channel in mtFabH (Figure 5A). We note that this flap includes an insertion sequence in mtFabH relative to ecFabH that mediates intersubunit interactions in the mtFabH dimer. The extremities of this polypeptide segment coincide with glycine residues (181 and 207) that are almost completely conserved across five FabH sequences. Synchronized hinge motions at each of these glycines could raise this polypeptide flap to expose most of the substrate binding site of mtFabH to solvent and to the binding of substrates and ligands (Figure 5). The proposed opening of this single flap in mtFabH is distinct from the disordered state of the unliganded ecFabH crystal structure (Qiu et al., 2001), in which four noncontiguous but proximal polypeptide loops that constitute much of the substrate binding site and dimer interface are not visible in the electron density map.

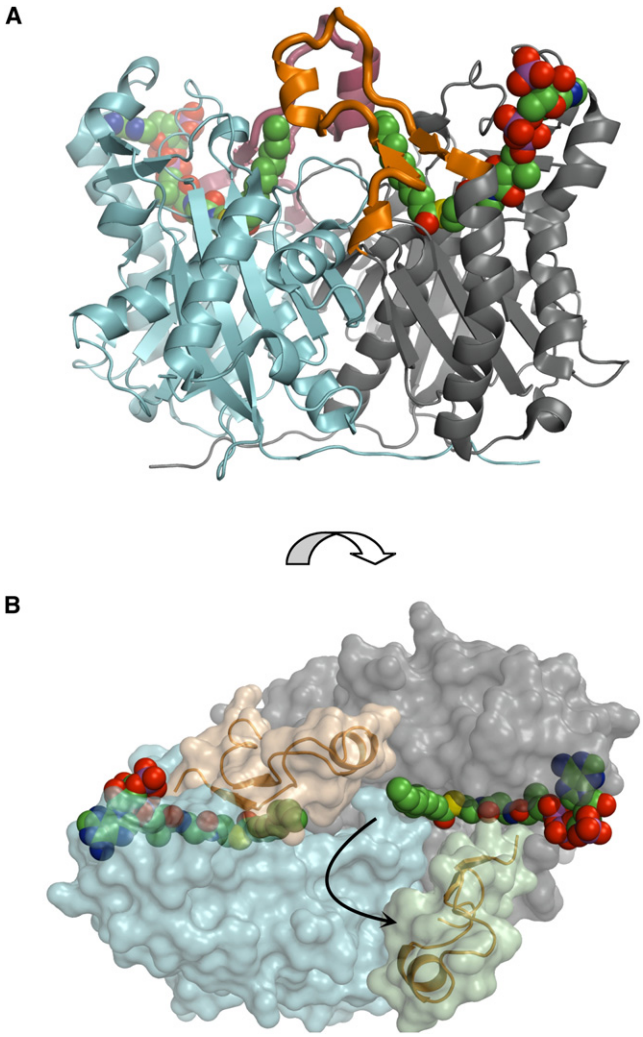

Figure 5. Proposed "Open" and "Closed" Structures of mtFabH

(A) Backbone ribbon model of the dimeric Cys112Ala mtFabH complex with lauroyl-CoA (color-coded space filling) bound in active sites of both monomers. The putative flap that covers the extended L-shaped binding site is colored gold (front) in the right-hand (gray) monomer and magenta (back) in the left-hand (blue) monomer subunit.

(B) Surface figure of the same dimer rotated ~90° about the horizontal axis showing the two flap covers (gold) of each of the two binding sites (defined by lauroyl-CoA color-coded space filling). The flap in the blue left monomer is in the closed conformation, thereby burying the lauroyl-CoA ligand; the flap in the gray right monomer is in the open conformation (movement shown by arrow), opening the lauroyl-CoA binding site to solvent.

This proposed open conformation of mtFabH provides an understanding of how both acyl-CoA substrates and the ligands **1–3** bind and react with the WT enzyme and how **1** reacts with the Ala246Phe mutant. The proposed open conformation of the mtFabH also offers a solution to the dilemma of how mtFabH utilizes substrates longer than palmitoyl-CoA (the maximum permitted chain length suggested by the closed mtFabH structure). Exposure of the acyl binding channel would allow longer chains

to extend outward from the channel, possibly interacting with the exposed hydrophobic underside of the distal end of the opened flap in a modified closed conformation of mtFabH that is necessarily slightly different from that observed with lauroyl-CoA substrate (Musayev et al., 2005). We propose that ordering or closing of the mtFabH on the substrate or inhibitor is required for efficient reaction with the active site cysteine, and that this is why **2** and **3** react poorly with the Ala246Phe mutant. Reaction of this mutant with **3** results in loss of fragment B″, whose only plausible position during this reaction is extended outward from the binding site, since the pantetheinate channel is blocked.

In this model for acyl-CoA binding to mtFabH, the acyl-CoA reactant, in principle, could synchronously bind to both arms of the exposed substrate binding site. Movement to the closed form, and reaction with Cys112, would follow. CoA product released from the mouth of the pantetheinate channel would then complete the first stage of the reaction. In the second stage of the mtFabH reaction, these different paths for substrate binding and product release would be reversed: the phosphopantetheine arm of ACP carrying the malonyl thioester would enter the mouth of the closed pantetheinate channel after CoA dissociation, and, following decarboxylative condensation of malonyl-ACP, would transition back to the open form of the enzyme to permit egress of the hydrophobic 3-ketoacyl ACP product. This open form could also facilitate transfer of the long, hydrophobic acyl chain from the acyl channel binding site of mtFabH to a putative binding site on ACP. This latter step is supported by kinetic analyses of the complete mtFabH reaction that indicate an apparent difference in acyl group specificity when using *E. coli* versus *M. tuberculosis* ACP (Brown et al., 2005), and by the structure of butyryl-ACP in which the acyl group is sequestered in a site on the ACP. In addition, we have observed ACP-dependent changes in substrate specificities of other FabH enzymes, and kinetic data for inhibition of ecFabH on binding a MeSSCoA inhibitor are consistent with conformational transitions on malonyl-ACP binding (Alhamadsheh et al., 2007).

SIGNIFICANCE

The *Mycobacterium tuberculosis* FabH (mtFabH) is proposed to be an important link between the type I and type II FAS (fatty acid synthase) responsible for mycolic acid biosynthesis. This work has demonstrated that large-scale dynamic motions in mtFabH are required for ligand binding. The data support a new model for catalysis, in which FabH exists in an "open" form that permits binding of the long chain acyl-coenzyme A substrate binding and release of the corresponding 3-ketoacyl ACP product. Catalysis and intermediate steps in the process are proposed to occur in a "closed" form of the mtFabH. These conformational changes may be critical for binding and dissociation steps in other enzymes of the FAS pathways, including transfers between the type I and type II FASII components of *M. tuberculosis*. Protein-protein interactions in these systems and the conformational changes of the individual proteins may offer alternative approaches in developing new therapeutics that target mycolic acid biosynthesis.

EXPERIMENTAL PROCEDURES

Synthesis of Inhibitors 1–3

Details of compound synthesis are described in the Supplemental Data available with this article online.

Enzyme Expression and Purification

Expression and purification of the WT mtFabH and Cys112Ala mtFabH have been described previously (Scarsdale et al., 2001; Musayev et al., 2005). The open reading frame Rv0533c (encoding the mtFabH) in the expression vector pET-15b (Scarsdale et al., 2001) was mutated with the Quikchange XL site-directed mutagenesis kit (Stratagene) to obtain an expression system for the Ala246Phe mtFabH mutant. Primers used were: 5′-GTG TTC GTC CCT CAT CAG TTC AAT AGC CGC ATC AAC GAG-3′ and 5′-CTC GTT GAT GCG GCT ATT GAA CTG ATG AGG GAC GAA CAC-3′. The appropriate mutation in the resulting pSSD1 plasmid was confirmed by sequencing. *E. coli* BL21DE3 Codon Plus cells (Novagen) were transformed with pSSD1 and the mtFabH mutant enzyme expressed and purified under the same conditions used for WT mtFabH. (Scarsdale et al., 2001; Musayev et al., 2005).

mtFabH Assays

mtFabH assays were carried out as previously described (Brown et al., 2005), substituting malonyl-CoA for malonyl-ACP.

Identification of Modified mtFabH Species by ESI-MS

WT and mutant mtFabHs in 50 mM sodium phosphate buffer, pH 7.0, 15% glycerol, were desalted with HPLC-grade water with a Hitrap desalting column (GE biosciences). An aliquot of enzyme (10–40 μM) and each of the inhibitors (**1**, **2**, and **3**) were incubated separately (at a 1:10 enzyme:inhibitor ratio) at room temperature for 60 min. Excess inhibitor was removed and the protein concentrated via sequential use of a desalting gel and a Microcon concentrator (50 kD cutoff). Protein samples stored at −20°C were thawed, diluted to a concentration of approximately 1 pm/μl with 50% methanol/0.1% formic acid, and analyzed by a quadrupole time-of-flight mass spectrometer (TOF/MS) (QSTAR XL; Applied Biosystems/MDS Sciex) equipped with a standard ion source (MDS Sciex). The instrument was externally calibrated in the positive ion mode with two fragment ion peaks (*m/z* 175.1190 and *m/z* 1285.5444) from the tandem mass spectrum of Glu-fibrinopeptide (Sigma). Samples were directly infused into the ion source with a 500 μl syringe at a flow rate of 5 μl/min. The following parameter settings were used to acquire mass spectra from *m/z* 600–1600 in the positive ion TOF/MS mode: spray voltage, 5500 V; GS1 gas, 15 l/hr; declustering potential (DP), 85 V; DP2, 15 V; focusing potential, 265 V; accumulation time, 1 s. Typically, spectra were averaged over 120 scans, and the series of multiply charged ion peaks were deconvoluted by the Bayesian protein reconstruct tool (in the Bioanalyst QS 1.1 software package) to determine the zero charge masses of the intact proteins. For all mass calculations, 0.01% mass accuracy was set as tolerance limit (<4 Da for mtFabH, the monomeric molecular of which weight is ~37,000).

Treatment of mtFabH with inhibitors **1–3** resulted in appearance of multiple novel species along with their sodium adducts (up to four sodium adducts were readily seen). The region of the most abundant species was identified, and all peaks with areas at least 10% of the most intense peak (species) were used for calculations. The mass value (36,903 Da) of untreated mtFabH control was subtracted from each mass value obtained, and the positive mass difference used to identify the species present. The relative areas of each peak (taking into account the various sodium adducts for each) were used to calculate the relative abundance of the species.

Crystallization, X-Ray Data Collection, and Structure Determination

Crystals were obtained by the hanging-drop vapor diffusion method with 4 μl drops consisting of a 1:1 ratio of protein:reservoir solution equilibrated against 600 μl of reservoir solution at room temperature. Protein concentration varied from 4 to 15 mg/ml in 100 mM sodium phosphate buffer, pH 7.0. Inhibitor molecules were dissolved in methanol to a final concentration of 34 mM (**1**), 25 mM (**2**), and 23 mM (**3**), and mixed with protein solution at the molar ratios shown in Table 1. Before crystallization, protein-inhibitor complex mixture was

Table 2. Data Collection and Refinement Statistic for mtFabH Crystal Structures

	Accession No.				
Statistics	2QNZ	2QNY	2QNX	2QO1	2QO0
Data Collection					
Resolution (Å)	48.38–2.30 (2.38–2.30)[a]	39.28–2.15 (2.23–2.15)	29.06–2.70 (2.80–2.70)	39.73–2.60 (2.69–2.60)	38.02–1.85 (1.92–1.85)
Unique reflections	31,228 (2987)	35,143 (2605)	19,219 (1913)	20,938 (2193)	46884 (4610)
Redundancy	12.43 (7.98)	3.17 (1.95)	3.65 (3.69)	2.54 (2.84)	6.37 (6.17)
R_{merge}[b]	0.089 (0.206)	0.075 (0.150)	0.120 (0.264)	0.108 (0.244)	0.095 (0.314)
Completeness (%)	99.3 (96.7)	92.2 (69.6)	97.3 (98.0)	93.2 (98.8)	99.8 (99.9)
I/σ (I)	19.6 (9.5)	10.7 (4.4)	8.7 (4.8)	7.4 (4.1)	11.3 (5.5)
Refinement					
Resolution (Å)	14.81–2.30 (2.38–2.30)	10.00–2.15 (2.20–2.15)	15.00–2.70 (2.77–2.70)	15.00–2.60 (2.67–2.60)	25.00–1.85 (1.90–1.85)
No. of reflections (work)	27,984 (1943)	31,289 (1625)	17,172 (1209)	18,707 (1459)	42064 (3050)
No. of reflections (test)	3115 (207)	3445 (182)	1954 (147)	2076 (146)	4710 (368)
R_{work}/R_{free}[c]	0.164/0.222 (0.192/0.257)	0.195/0.245 (0.215/0.273)	0.209/0.254 (0.294/0.347)	0.221/0.298 (0.287/0.358)	0.194/0.264 (0.314/0.371)
Average B ($Å^2$)	28.9	30.2	26.8	40.5	22.9
DPI (Å)[d]	0.212	0.213	0.352	0.389	0.162
Deviations from ideality					
Bond lengths (Å)	0.007	0.007	0.007	0.007	0.009
Bond angles (deg)	1.11	1.08	1.11	1.1	1.22
Ramachandran plot (%)					
Most favored	90.7	90.1	88.1	88.8	90.5
Additional allowed	9.0	9.1	11.3	10.4	9.0
Generously allowed	0.2	0.4	0.4	0.5	0.4
Forbidden	0.2	0.4	0.2	0.4	0.2

[a] Values in parentheses are for highest resolution shell.
[b] $R_{merge} = \sum |I_h - \langle I \rangle| / \langle I \rangle$, where I_h refers to the measured intensity for a given reflection and <I> refers to the average measured intensity for that reflection.
[c] $R_{work} = \sum |F_{obs} - F_{calc}| / \sum F_{obs}$, where F_{obs} and F_{calc} refer to the observed and calculated structure factors, respectively.
[d] $DPI = (N_{atoms}/N_{obs})^{1/2} c^{-1/3} d_{min} R_{free}$, where N_{atoms} is the number of atoms in the refinement, N_{obs} is the number of reflections, c is the data set completeness expressed as a fraction, d_{min} is the resolution and R_{free} is the free R factor.

incubated on ice for 2 hr. Crystallization conditions and lattice parameters for the structures determined are summarized in Table 1.

For X-ray data collection, crystals were cryoprotected in their mother liquid solution supplemented with 25%–30% glycerol, and, where appropriate, inhibitors, before flash cooling in a liquid nitrogen stream. X-ray data were collected at 100K with a Molecular Structure Corporation (MSC) X-Stream Cryogenic Crystal Cooler System and an R-Axis IV++ image plate detector with a Rigaku MicroMax-007 X-ray source equipped with MSC Varimax confocal optics operating at 40 kV and 20 mA. Data were processed and scaled with D*Trek (Pflugrath, 1999). Structures were determined via molecular replacement with AMORE (Navaza, 1994), with PDB entry 1HZP (Scarsdale et al., 2001) as a search model, and refined via alternating cycles of manual fitting into SigmaA weighted $2mf_o df_c$ maps in COOT (Emsley and Cowtan, 2004) and computational refinement in CNS (Brunger et al., 1998) and Refmac5 (Murshudov et al., 1999). Ligand topology and parameter files used in refinement were generated with the PRODRG server (Schuettelkopf and van Aalten, 2004). Data collection and refinement statistics are summarized in Table 2.

ACCESSION NUMBERS

Structures have been deposited to the RCSB under ID codes 2QNZ, 2QNY, 2QNX, 2QO1, and 2QO0.

SUPPLEMENTAL DATA

Supplemental Data, including Supplemental Experimental Procedures used in this work, are available online at http://www.chembiol.com/cgi/content/full/15/4/402/DC1/.

ACKNOWLEDGMENTS

We thank Major Norman Waters and the Walter Reed Army Institute for Research for apprising us of their work on linear disulfide inhibitors for the *Plasmodial falciparum* FabH. This work was supported by grant AI52230 from the National Institutes of Health.

Received: October 16, 2007
Revised: March 3, 2008
Accepted: March 5, 2008
Published: April 18, 2008

REFERENCES

Alhamadsheh, M.M., Musayev, F., Komissarov, A.A., Sachdeva, S., Wright, H.T., Scarsdale, J.N., Florova, G., and Reynolds, K.A. (2007). Alkyl-CoA

disulfides as inhibitors and mechanistic probes for FabH enzymes. Chem. Biol. *14*, 513–524.

Asselineau, C., Asselineau, J., Laneelle, G., and Laneelle, M.A. (2002). The biosynthesis of mycolic acids by mycobacteria: current and alternative hypotheses. Prog. Lipid Res. *41*, 501–523.

Bhatt, A., Molle, V., Besra, G.S., Jacobs, W.R., Jr., and Kremer, L. (2007). The *Mycobacterium tuberculosis* FAS-II condensing enzymes: their role in mycolic acid biosynthesis, acid-fastness, pathogenesis and in future drug development. Mol. Microbiol. *64*, 1442–1454.

Brown, A.K., Bhatt, A., Singh, A., Saparia, E., Evans, A.F., and Besra, G.S. (2007). Identification of the dehydratase component of the mycobacterial mycolic acid-synthesizing fatty acid synthase-II complex. Microbiology *153*, 4166–4173.

Brown, A.K., Sridharan, S., Kremer, L., Lindenberg, S., Dover, L.G., Sacchettini, J.C., and Besra, G.S. (2005). Probing the mechanism of the *Mycobacterium tuberculosis* β-ketoacyl-acyl carrier protein synthase III mtFabH: factors influencing catalysis and substrate specificity. J. Biol. Chem. *280*, 32539–32547.

Brunger, A.T., Adams, P.D., Clore, G.M., DeLano, W.L., Gros, P., Grosse-Kunstleve, R.W., Jiang, J.S., Kuszewski, J., Nilges, M., Pannu, N.S., et al. (1998). Crystallography & NMR system: a new software suite for macromolecular structure determination. Acta Crystallogr. D Biol. Crystallogr. *54*, 905–921.

Choi, K.H., Heath, R.J., and Rock, C.O. (2000a). β-Ketoacyl-acyl carrier protein synthase III (FabH) is a determining factor in branched-chain fatty acid biosynthesis. J. Bacteriol. *182*, 365–370.

Choi, K.H., Kremer, L., Besra, G.S., and Rock, C.O. (2000b). Identification and substrate specificity of β-ketoacyl (acyl carrier protein) synthase III (mtFabH) from *Mycobacterium tuberculosis*. J. Biol. Chem. *275*, 28201–28207.

Cohen-Gonsaud, M., Ducasse-Cabanot, S., Quemard, A., and Labesse, G. (2005). Ligand-induced fit in mycobacterial MabA: the sequence-specific C-terminus locks the conformational change. Proteins *60*, 392–400.

Cohen-Gonsaud, M., Ducasse, S., Hoh, F., Zerbib, D., Labesse, G., and Quemard, A. (2002). Crystal structure of MabA from *Mycobacterium tuberculosis*, a reductase involved in long-chain fatty acid biosynthesis. J. Mol. Biol. *320*, 249–261.

Emsley, P., and Cowtan, K. (2004). Coot: model-building tools for molecular graphics. Acta Crystallogr. D Biol. Crystallogr. *60*, 2126–2132.

Han, L., Lobo, S., and Reynolds, K.A. (1998). Characterization of β-ketoacyl-acyl carrier protein synthase III from *Streptomyces glaucescens* and its role in initiation of fatty acid biosynthesis. J. Bacteriol. *180*, 4481–4486.

Jarlier, V., and Nikaido, H. (1994). Mycobacterial cell wall: structure and role in natural resistance to antibiotics. FEMS Microbiol. Lett. *123*, 11–18.

Jenni, S., Leibundgut, M., Boehringer, D., Frick, C., Mikolasek, B., and Ban, N. (2007). Structure of fungal fatty acid synthase and implications for iterative substrate shuttling. Science *316*, 254–261.

Larsen, M.H., Vilcheze, C., Kremer, L., Besra, G.S., Parsons, L., Salfinger, M., Heifets, L., Hazbon, M.H., Alland, D., Sacchettini, J.C., and Jacobs, W.R., Jr. (2002). Overexpression of InhA, but not KasA, confers resistance to isoniazid and ethionamide in *Mycobacterium smegmatis*, *M. bovis* BCG and *M. tuberculosis*. Mol. Microbiol. *46*, 453–466.

Lomakin, I.B., Xiong, Y., and Steitz, T.A. (2007). The crystal structure of yeast fatty acid synthase, a cellular machine with eight active sites working together. Cell *129*, 319–332.

Lu, Y.J., Zhang, Y.M., and Rock, C.O. (2004). Product diversity and regulation of type II fatty acid synthases. Biochem. Cell Biol. *82*, 145–155.

Murshudov, G.N., Vagin, A.A., Lebedev, A., Wilson, K.S., and Dodson, E.J. (1999). Efficient anisotropic refinement of macromolecular structures using FFT. Acta Crystallogr. D Biol. Crystallogr. *55*, 247–255.

Musayev, F., Sachdeva, S., Scarsdale, J.N., Reynolds, K.A., and Wright, H.T. (2005). Crystal structure of a substrate complex of *Mycobacterium tuberculosis* β-ketoacyl-acyl carrier protein synthase III (FabH) with lauroyl-coenzyme A. J. Mol. Biol. *346*, 1313–1321.

Navaza, J. (1994). AMoRe: an automated package for molecular replacement. Acta Crystallogr. A *50*, 157–163.

Nikaido, H., and Jarlier, V. (1991). Permeability of the mycobacterial cell wall. Res. Microbiol. *142*, 437–443.

Pflugrath, J.W. (1999). The finer things in X-ray diffraction data collection. Acta Crystallogr. D Biol. Crystallogr. *55*, 1718–1725.

Portevin, D., De Sousa-D'Auria, C., Houssin, C., Grimaldi, C., Chami, M., Daffe, M., and Guilhot, C. (2004). A polyketide synthase catalyzes the last condensation step of mycolic acid biosynthesis in mycobacteria and related organisms. Proc. Natl. Acad. Sci. USA *101*, 314–319.

Qiu, X., Janson, C.A., Smith, W.W., Head, M., Lonsdale, J., and Konstantinidis, A.K. (2001). Refined structures of β-ketoacyl-acyl carrier protein synthase III. J. Mol. Biol. *307*, 341–356.

Rozwarski, D.A., Grant, G.A., Barton, D.H., Jacobs, W.R., Jr., and Sacchettini, J.C. (1998). Modification of the NADH of the isoniazid target (InhA) from *Mycobacterium tuberculosis*. Science *279*, 98–102.

Sacco, E., Covarrubias, A.S., O'Hare, H.M., Carroll, P., Eynard, N., Jones, T.A., Parish, T., Daffe, M., Backbro, K., and Quemard, A. (2007a). The missing piece of the type II fatty acid synthase system from *Mycobacterium tuberculosis*. Proc. Natl. Acad. Sci. USA *104*, 14628–14633.

Sacco, E., Legendre, V., Laval, F., Zerbib, D., Montrozier, H., Eynard, N., Guilhot, C., Daffée, M., and Quéemard, A. (2007b). Rv3389C from *Mycobacterium tuberculosis*, a member of the (R)-specific hydratase/dehydratase family. Biochim. Biophys. Acta *1774*, 303–311.

Scarsdale, J.N., Kazanina, G., He, X., Reynolds, K.A., and Wright, H.T. (2001). Crystal structure of the *Mycobacterium tuberculosis* β-ketoacyl-acyl carrier protein synthase III. J. Biol. Chem. *276*, 20516–20522.

Schuettelkopf, A.J., and van Aalten, D.M.F. (2004). PRODRG—a tool for high-throughput crystallography of protein-ligand complexes. Acta Crystallogr. D Biol. Crystallogr. *60*, 1355–1363.

Sridharan, S., Wang, L., Brown, A.K., Dover, L.G., Kremer, L., Besra, G.S., and Sacchettini, J.C. (2007). X-ray crystal structure of *Mycobacterium tuberculosis* β-ketoacyl acyl carrier protein synthase II (mtKasB). J. Mol. Biol. *366*, 469–480.

Takayama, K., Wang, C., and Besra, G.S. (2005). Pathway to synthesis and processing of mycolic acids in *Mycobacterium tuberculosis*. Clin. Microbiol. Rev. *18*, 81–101.

Veyron-Churlet, R., Bigot, S., Guerrini, O., Verdoux, S., Malaga, W., Daffe, M., and Zerbib, D. (2005). The biosynthesis of mycolic acids in *Mycobacterium tuberculosis* relies on multiple specialized elongation complexes interconnected by specific protein-protein interactions. J. Mol. Biol. *353*, 847–858.

Veyron-Churlet, R., Guerrini, O., Mourey, L., Daffe, M., and Zerbib, D. (2004). Protein-protein interactions within the fatty acid synthase-II system of *Mycobacterium tuberculosis* are essential for mycobacterial viability. Mol. Microbiol. *54*, 1161–1172.

Wong, H.C., Liu, G., Zhang, Y.M., Rock, C.O., and Zheng, J. (2002). The solution structure of acyl carrier protein from *Mycobacterium tuberculosis*. J. Biol. Chem. *277*, 15874–15880.

